https://doi.org/10.5194/egusphere-2026-4881
Preprint. Discussion started: 19 August 2026

Furfural Exhibits Distinct Photooxidation and Secondary Organic Aerosol Formation Among Biomass Burning Related Furanoids

Taekyu Joo[1,2], David Pando[3], Jo E. Machesky[4,*], Tori Hass-Mitchell[4,**], Jean C. Rivera-Rios[3,***], Drew R. Gentner[4], Matthew J. Alvarado[5], Nga L. Ng[2,3,6,7]

[1]Department of Earth and Environmental Sciences, Korea University, Seoul, 02841, South Korea

[2]School of Earth and Atmospheric Sciences, Georgia Institute of Technology, Atlanta, Georgia, 30332, USA

[3]School of Chemical and Biomolecular Engineering, Georgia Institute of Technology, Atlanta, G eorgia, 30332, USA

[4]Department of Chemical and Environmental Engineering, Yale University, New Haven, Connecticut, 06511, USA

[5]Atmospheric and Environmental Research, JANUS Research Group, Lexington, Massachusetts, 02421, USA

[6]School of Civil and Environmental Engineering, Georgia Institute of Technology, Atlanta, Georgia, 30332, USA

[7]Division of Engineering and Applied Science, California Institute of Technology, California 91125, USA

*Now at Environmental Protection Agency, Durham, North Carolina, 27703, USA

**Now at City of Boston, Boston, Massachusetts, 02201, USA

***Now at Department of Chemistry and Chemical Biology, Rutgers University, New Brunswick, New Jersey, 08854, USA

Correspondence to: Taekyu Joo (taekyujoo@korea.ac.kr) and Nga L. Ng (ng@caltech.edu)

Abstract. Furanoids are a major compound class emitted during biomass burning and are highly reactive toward hydroxyl radicals (OH), suggesting their oxidation may contribute to secondary organic aerosol (SOA) formation. Previous furanoid studies focused on gas-phase kinetics, leaving SOA

https://doi.org/10.5194/egusphere-2026-4881
Preprint. Discussion started: 19 August 2026

formation poorly understood. Here, we investigate the gas-phase oxidation and SOA formation from furfural, 2-methylfuran, and 3-methylfuran reactions with OH radicals in the presence of nitrogen oxides at RH<5%. Furfural exhibits distinct oxidation chemistry compared with methylfurans: furfural alkyl radical preferentially reacts with NO_2, whereas methylfuran oxidation proceeds via peroxy radical (RO_2)+NO channel to form alkoxy radicals. Methylfuran isomers also differ in oxidation product speciation, with 2-methylfuran generating C_4 and C_5 compounds, whereas 3-methylfuran predominantly forms C_5 compounds. $C_4H_2O_3$, potentially maleic anhydride, increases continuously during all furanoid oxidations, supporting its potential as an aged biomass burning marker. Furfural produces the highest SOA mass and yield (66.3 $\mu g \cdot m^{-3}$, 9.8%), followed by 2-methylfuran (10.3 $\mu g \cdot m^{-3}$, 1.4%) and 3-methylfuran (7.2 $\mu g \cdot m^{-3}$, 1.1%). Compared with methylfuran SOA, furfural SOA shows stronger signatures of lower-volatility oligomers, with higher contributions from large *m/z* fragments, a greater degree of unsaturation, broader thermograms, and more reduced CHON species (O/N<3). Accordingly, estimated particulate organic nitrate fraction is highest for 2-methylfuran SOA (~45%), followed by 3-methylfuran (~36%) and furfural (~11%). These results show that both substituent type and position should be considered when representing furanoid oxidation in atmospheric models.

1 Introduction

Biomass burning is a significant source of particulate matter (PM) and volatile organic compounds (VOCs) in the atmosphere (Crutzen and Andreae, 1990; Akagi et al., 2011; Reddington et al., 2016; Stockwell et al., 2015). It influences air quality, public health, and climate and is expected to increase due to climate change, affecting broad regions from local to continental scale (Abatzoglou and Williams, 2016; Burke et al., 2023; Joo et al., 2024b). Thousands of different VOCs are released to the atmosphere from biomass burning. They can react with atmospheric oxidants such as hydroxyl (OH) and nitrate (NO_3) radicals to form secondary pollutants such as ozone and secondary organic aerosol (SOA) (Alvarado et al., 2015; Alvarado and Prinn, 2009), which are reported to have detrimental health effects (Pye et al., 2021; Liu et al., 2023; Joo et al., 2024b; Pardo et al., 2024; Daellenbach et al., 2020; Zhou et al., 2019). Recent laboratory combustion studies revealed that SOA formation from biomass burning VOCs can be substantial (Fang et al., 2017; Lim et al., 2019), and that more than 80% of SOA can come

https://doi.org/10.5194/egusphere-2026-4881
Preprint. Discussion started: 19 August 2026

from less-studied precursors (Grieshop et al., 2009). Among the non-traditional VOCs, oxygenated aromatic compounds (e.g., phenols) and heterocyclic compounds (e.g., furanoids) generally have higher emissions in smoldering combustion than flaming combustion (Jen et al., 2019) and have been reported to have high SOA formation potential (Bruns et al., 2016; Hatch et al., 2017; Stefenelli et al., 2019; Akherati et al., 2020).

Furanoids are generated as a result of the pyrolysis of cellulose (Mettler et al., 2012; Romanias et al., 2024) and their contribution to total VOC emissions and subsequent SOA formation potential is reported to be particularly significant from combustion of grass- or straw-type fuel (Hatch et al., 2017; Stefenelli et al., 2019; Akherati et al., 2020). Once released into atmosphere, furanoids are highly reactive with atmospheric oxidants, contributing 9–25% of total OH radical reactivity among VOCs emitted from combustion of biomass fuels widely distributed across the United States (Koss et al., 2018; Gilman et al., 2015; Decker et al., 2021) and 18–23% of total NO_3 radical reactivity for VOCs emitted from rice straw and ponderosa pine combustion (Decker et al., 2019). The oxidation of furanoids by atmospheric oxidants can generate multi-functional oxidation products. Specifically, the formation yield of unsaturated multi-carbonyls has been reported to range from 8 to 75% (Aschmann et al., 2014; Gómez Alvarez et al., 2009; Bierbach et al., 1995). Such products containing one or more functionalities have multiple reactive sites that can trigger further accretion reactions to generate semi-volatile or low-volatility organic compounds (SVOCs or LVOCs) (Kroll and Seinfeld, 2008; Ziemann and Atkinson, 2012; Joo et al., 2019), resulting in the formation of SOA with yields of 0.03–15% (for an OA mass concentration of 1.0–4900 μg m^{-3}) (Romanias et al., 2024; Jiang et al., 2019; Gómez Alvarez et al., 2009; Strollo and Ziemann, 2013; Colmenar et al., 2020; Tajuelo et al., 2021).

Recently, the increasing prevalence of wildfires globally and their significant contributions to secondary atmospheric chemistry have driven substantial research on the oxidation of furanoids by various atmospheric oxidants. Despite these efforts, studies on SOA formation from furanoid photooxidation have thus far lacked continuous, real-time measurements of both gas- and particle-phase chemical composition (Romanias et al., 2024; Strollo and Ziemann, 2013; Al Ali et al., 2024; Jiang et al., 2019; Gómez Alvarez et al., 2009; Colmenar et al., 2020; Schueneman et al., 2024; Tajuelo et al., 2021). This limitation hinders a comprehensive understanding of the detailed gas-phase oxidation

https://doi.org/10.5194/egusphere-2026-4881
Preprint. Discussion started: 19 August 2026

chemistry and the corresponding SOA formation potential. Moreover, many investigations have primarily focused on reaction kinetics and reactivity with atmospheric oxidants (Bierbach et al., 1995; Zhao and Wang, 2017; Aschmann et al., 2014, 2011; Jiang et al., 2020; Tapia et al., 2011; Yuan et al., 2017), with relatively few examining the chemical mechanisms and SOA yields (Romanias et al., 2024).

In this work, we investigated SOA formation from photooxidation of furanoids in the presence of nitrogen oxides (NO_x), focusing on 2-furaldehyde (furfural), 2-methylfuran, and 3-methylfuran, which together account for 58–67% of furanoids emitted from biomass burning (Hatch et al., 2017; Akagi et al., 2011; Gilman et al., 2015; Ciccioli et al., 2001). The composition of gas- and particle-phase products are characterized using online measurements, and the mechanisms for multigenerational gas-phase oxidation and particle-phase reactions are proposed. The results provide new insights into the photooxidation chemistry of furanoids and can improve the representation of SOA formation and evolution in biomass burning plumes in atmospheric models.

2 Methods

2.1 Environmental Chamber Experiments

Experiments are performed at 22 ℃ under dry (<5 % RH) conditions in the Georgia Tech Environmental Chamber (GTEC) facility which consists of two 12 m^3 Teflon chambers (Boyd et al., 2015). The chamber is cleaned for a day prior to each experiment with pure air (747-14, Aadco, Cleves, OH) at a rate of 35 L min^{-1}. Ammonium sulfate seed aerosol is introduced into the chamber by atomizing a 0.015M solution for 20 min and passing through a neutralizer. The initial seed particle number and volume concentrations are ~20000 particles cm^{-3} and ~20 μm^3 cm^{-3}, respectively. A similar initial amount of 2-furaldehyde (furfural, 99%, Sigma-Aldrich, St. Louis, MO), 2-methylfuran (99%, Sigma-Aldrich), or 3-methylfuran (98%, ACROS, Geel, Belgium) is injected into a pure air-flowing glass bulb for introducing the precursor VOC into the chamber for quantitative comparison of SOA formation. Nitrous acid (HONO) is injected as an OH source, which has been reported as an important source of OH in wildfire plumes (Palm et al., 2020; Peng et al., 2020). HONO is generated following the procedure described in Tuet et al. (2017): adding 10 mL of 1% wt aqueous $NaNO_2$ (VWR International,

https://doi.org/10.5194/egusphere-2026-4881
Preprint. Discussion started: 19 August 2026

Radnor, PA) dropwise into 20 mL of 10% wt H_2SO_4 (VWR International) in a glass bulb and then passing zero air over the solution to introduce HONO into the chamber. The HONO injection line is flushed for 5 min after the injection and then irradiation of UV black lights initiated photooxidation. Photolysis of HONO yields 6×10^6–2×10^7 molecules cm^{-3} of OH radicals. NO and NO_2 are also formed during the HONO synthesis as byproducts. The photolysis rate of NO_2 (j_{NO2}) in the chamber is ~0.2 min^{-1}.

2.2 Instrumentation and data analysis

Online bulk aerosol chemical composition is measured using a high-resolution time-of-flight aerosol mass spectrometer (HR-ToF-AMS, Aerodyne Research Inc., Billerica, MA). HR-ToF-AMS quantifies organics, nitrate, sulfate, ammonium, and chloride mass concentrations and measures the bulk elemental composition of organics (e.g., O:C and H:C ratios) (Aiken et al., 2007; Decarlo et al., 2006; Canagaratna et al., 2015). The data analysis is performed using SQUIRREL v1.57G and PIKA v1.16G in Igor Pro 6.38B01. Gas- and particle-phase molecular-level compositions are measured and reported as counts per second using a high-resolution time-of-flight chemical ionization mass spectrometer (HR-ToF-CIMS, Aerodyne Research Inc.) coupled with a Filter Inlet for Gases and AEROsol (FIGAERO, Aerodyne Research Inc.) inlet system (Nah et al., 2016a; Lopez-Hilfiker et al., 2014). Iodide (I^-) is used as a reagent ion, which selectively measures polar or acidic compounds, and detected signals are normalized by I^- (Aljawhary et al., 2013). FIGAERO-CIMS data analysis is performed in Igor Pro 6.38B01 (WaveMetrics Inc.) using Tofware v2.5.11. The general operation detail of FIGAERO-CIMS has been described in a previous study (Nah et al., 2016a). Briefly, reagent ions are introduced into the ion-molecular reaction (IMR) chamber as a mixture of methyl iodide (CH_3I) and dry ultrahigh purity (UHP) N_2 (Airgas) that is passed through a ^{210}Po radioactive source (model P-2021, NRD, Grand Island, NY). As sensitivity can decrease if the amount of reagent ion depletes substantially and/or secondary chemistry in IMR occurs (Lee et al., 2014), the gas sampling line is diluted with zero air before the inlet to keep the fraction of I^- to the total ions above 80%. To prevent fluctuations in the sensitivity, we follow the specific setting described in Takeuchi and Ng (2019) that humidify the IMR with humidified N_2 to minimize variation of the iodide ion chemistry that could arise from difference

https://doi.org/10.5194/egusphere-2026-4881
Preprint. Discussion started: 19 August 2026

in water vapor pressure in each experiment (Lee et al., 2014). While measuring gas-phase species, particles are collected onto a PTFE filter (Pall Corp, Zefluor 25 mm, 2 µm pore-size) in FIGAERO for 20 min and the particle-phase composition is analyzed through thermal desorption cycle (40 min total, including temperature ramping, soaking, and cooling cycle). We further obtain volatility distribution of OA as saturation mass concentration (C*, µg m^{-3}) via calibration procedure using compounds of known vapor pressures and matching to their desorption temperature corresponding to the signal peak (T_{max}) (Stark et al., 2017). The estimation of C* is detailed in Joo et al. (2019).

Offline bulk aerosol composition is analyzed using a liquid chromatography coupled with electrospray ionization and high-resolution quadrupole time-of-flight tandem mass spectrometry (LC-ESI-Q-ToF, Agilent 1260 Infinity LC and Agilent 6550 Q-ToF, Agilent, Santa Clara, CA). Additional chamber experiments (Table S1) with higher initial VOC concentrations are performed to facilitate collection of sufficient aerosol mass via filter sampling (47 mm Teflon filter, 2 µm pore size, Pall Corporation) to increase detected ion abundances across a greater range of analytes and thus reduce analytical uncertainties. Agilent Poroshell 120 SB-Aq reverse-phase column (2.1 × 50 mm, 2.7 µm particle size) is used for LC, and the analysis is performed in both positive and negative modes. Details of filter extractions, data acquisition, non-targeted data analysis, and QA/QC are discussed previously (Ditto et al., 2018). Formulas are assigned for the ions in range of *m/z* 50 – 600 assuming $[M + H]^+$, $[M + Na]^+$, and $[M + NH_4]^+$ addition in ESI positive mode, $[M\text{-}H]^-$ and $[M + HCOO]^-$ or $[M + CH_3COO]^-$ in negative mode, and also neutral water loss. Ions that surpassed instrument noise (isotope height of 1000 counts and compound height of 5000 counts) and strong peak quality score are assigned with the following elemental constraints ($C_{1\text{-}60}H_{0\text{-}120}O_{0\text{-}30}N_{0\text{-}5}S_{0\text{-}1}$) in Agilent's MassHunter software.

Size-dependent particle number and volume concentrations are monitored using a scanning mobility particle sizer (SMPS). The SMPS consists of a differential mobility analyzer (DMA) (TSI 3040, TSI Inc., Shoreview, MN) and a condensation particle counter (CPC) (TSI 3775). SMPS is operated under low-flow mode with sheath flow of 2 L min^{-1} to scan particles up to 1 µm size range. Precursor VOC concentration is monitored using a gas chromatograph-flame ionization detector (GC-FID, Agilent 7890A, Agilent, Santa Clara, CA) with a PLOT-Q column (Agilent). NO, and NO_2 are monitored using a chemiluminescence NO-NO_2-NO_x Analyzer (42C, Thermo Fisher Scientific,

https://doi.org/10.5194/egusphere-2026-4881
Preprint. Discussion started: 19 August 2026

Waltham, MA) and a cavity attenuated phase shift NO_2 monitor (CAPS, Aerodyne Research Inc.), respectively.

3 Results

3.1 SOA formation from OH radical oxidation of furanoids

Table 1 summarizes furanoid SOA formation experiments that are performed in this study. The particle wall-loss-corrected SOA yield of furanoid photooxidation range from 1.1% to 9.8% for an organic aerosol mass concentration (ΔM_o) of 7.2 to 66.3 μg m^{-3}, with the highest SOA yield and ΔM_o observed in the furfural+OH experiment among the examined furanoids. ΔM_o is estimated by converting SMPS volume concentration to aerosol mass concentration using the SOA density, which is determined by performing a series of nucleation experiments. By comparing mobility and aerodynamic diameters measured by SMPS and HR-ToF-AMS, respectively (Bahreini et al., 2005), the SOA density for furfural SOA, 2-methylfuran SOA, and 3-methylfuran SOA, is estimated to be 1.35 g cm^{-3}, 1.42 g cm^{-3}, and 1.40 g cm^{-3}, respectively.

There are a few studies to date that have quantified SOA formation from furfural+OH, 2-methylfuran+OH, and 3-methylfuran+OH (Figure S1). Schueneman et al. (2024) reported an SOA yield of 16% for ΔM_o = 100 μg m^{-3}, and Strollo and Ziemann (2013) reported SOA yields of 12 and 15% for ΔM_o = 2000 and 4900 μg m^{-3} in furfural and 3-methylfuran photooxidation experiments, respectively. Meanwhile, Colmenar et al. (2020) reported a substantially lower SOA yield (0.3% for ΔM_o = 90 μg m^{-3}) from the photooxidation of furfural, which could arise from vapor wall loss processes (Nah et al., 2016b; Zhang et al., 2014) as the experiments were conducted without seed particles. Even within this limited set of available studies, and despite their varying results, furfural SOA yields are generally higher than those reported for 3-methylfuran SOA, highlighting the need for systematic comparison of SOA formation across individual furanoids under controlled experimental conditions to better constrain their contribution to SOA formation from biomass burning emissions.

https://doi.org/10.5194/egusphere-2026-4881
Preprint. Discussion started: 19 August 2026

3.2 Chemical composition of gas- and particle-phase components

3.2.1 Evolution of gas-phase species during photooxidation of furanoids

Temporal variations of NO and NO_2 during furanoid+OH reaction are shown in Figure 1a, c, and e. While 2- and 3-methylfuran experiments show rapid NO decay and depletion of parent VOCs accompanied by a sharp increase in NO_2 once oxidation is initiated, furfural experiment exhibits a much slower NO decay and even a slight NO increase at the reaction onset. Temporal profiles of the precursor VOCs likewise differ by furanoids: 2- and 3-methylfuran are depleted within 50 min of oxidation (Figure 1d and f), whereas furfural declines steadily until the end of the experiment (Figure 1b). This behavior is consistent with the slower reaction rate of furfural+OH compared to 2- and 3-methylfuran+OH (Bierbach et al., 1995; Coggon et al., 2019), although the observed decay could also reflect differences in effective OH exposure of the parent VOCs.

A subset of gas-phase oxidation products that are sensitive to iodide reagent ion is identified using HR-ToF-CIMS (Figure S2). While the most prominent compound detected during both furfural and 2-methylfuran experiments share the same *m/z* and molecular formula (*m/z* 100, $C_4H_4O_3$), the two systems show distinct product speciation. For OH oxidation of furfural, the dominant gas-phase products are primarily CHO compounds, whereas the 2-methylfuran system also produces notable CHON species (i.e., $C_4H_3NO_5$, $C_5H_5NO_5$). Overall, CHON species account for a higher fraction of total gas-phase signal in the 2-methylfuran experiment (20%) compared to the furfural experiment (10%), where 8% and 2% come from CHON species with O/N ≥3 and O/N<3 in the furfural experiment, respectively. Meanwhile, the gas-phase signal during the 3-methylfuran experiment is dominated by $C_5H_6O_3$ (*m/z* 114), with the total signal from remaining identified compounds measured at less than 15% of the $C_5H_6O_3$ signal.

Temporal variations of the selected gas-phase oxidation products (Figure 1b, d, and f) can be grouped into three categories: (1) first-generation product characteristics, showing an immediate increase at the onset of oxidation; (2) a slower increase compared to first-generation products, reaching the maximum signal within 200 min after the initiation of oxidation; and (3) compounds that continue to increase until the end of the experiment. $C_5H_4O_3$ (*m/z* 112) generated during furfural oxidation (Figure 1b), $C_4H_4O_3$ (*m/z* 100) and $C_5H_6O_3$ (*m/z* 114) generated during 2-methylfuran oxidation (Figure

https://doi.org/10.5194/egusphere-2026-4881
Preprint. Discussion started: 19 August 2026

1d), and $C_5H_6O_3$ (*m/z* 114) generated during 3-methylfuran oxidation (Figure 1f) can be classified as the first-generation products. Most of the other detected species fall into the second category, and only CH_2O_2 (*m/z* 46) shows a continuous increase until the end of the experiment across all systems.

3.2.2 Chemical composition of furanoid SOA

Typical mass spectra of furanoid SOA obtained via HR-ToF-AMS are shown in Figure 2. Furfural SOA exhibits three distinctive characteristics among furanoid SOA examined in this study. Firstly, signals at *m/z* above 50 are observed to account for 14% of furfural SOA, which is ~3 times higher than that of 2- and 3-methylfuran SOA. Secondly, fraction of *m/z* 43 ($C_2H_3O^+$) to OA (f_{C2H3O+}) of furfural SOA is ~5 times lower compared to 2- and 3-methylfuran SOA. In contrast, a well-known organic acid indicator, the *m/z* 44 (CO_2^+) to OA (f_{CO2+}) ratio (Alfarra et al., 2004; Ng et al., 2011), remains similar among all furanoid SOA, ranging from 21 to 25%. Lastly, a prominent signal at *m/z* 96 ($C_5H_4O_2^+$), which corresponds to the molecular weight of furfural, is found exclusively in furfural SOA. Given the absence of enhanced signals at *m/z* 82 ($C_5H_6O^+$, methylfuran parent ion) in 2- and 3-methylfuran SOA, the oligomers in furfural SOA may retain the structure of the parent compound, unlike the oligomers that compose 2- and 3-methylfuran SOA.

Speciated composition of furanoid SOA identified using FIGAERO-CIMS is shown as mass spectra at the peak SOA mass concentration in Figure S3. $C_5H_4O_4$, $C_4H_4O_3$, and $C_5H_6O_3$, which are also observed with elevated signals in the gas-phase mass spectra (Figure S2), exhibit the strongest signal levels in furfural, 2-methylfuran, and 3-methylfuran SOA, respectively. Besides these major species, furfural and 2-methylfuran SOA show higher signal levels across various $C_{4\text{-}5}$ compounds, whereas 3-methylfuran SOA is dominated by C_5 compounds. These observations are consistent with gas-phase species speciation (Figure S2), where furfural and 2-methylfuran systems show substantial contributions from both C_4 and C_5 compounds (e.g., $C_4H_4O_3$, $C_5H_4O_4$, $C_5H_6O_3$) while the 3-methylfuran system is dominated by $C_5H_6O_3$. Considering that FIGAERO-CIMS uses thermal desorption technique to probe particle-phase composition, the detected particulate $C_{4\text{-}5}$ compounds may include fragments produced by thermal decomposition of oligomers.

https://doi.org/10.5194/egusphere-2026-4881
Preprint. Discussion started: 19 August 2026

Besides the CHO species that show stronger signal intensity across the furanoid SOA examined in this study, only a few CHON species such as $C_5H_3NO_5$, $C_4H_5NO_7$, $C_5H_7NO_7$ show higher signals among the identified CHON components. Figure 3 summarizes the relative abundances of identified compounds by carbon number and oxygen number, grouped into CHO and CHON compound classes. $C_{4\text{-}5}$ compounds in furanoid SOA are mostly composed of CHO species with 3 to 6 oxygen atoms. However, CHON species in 2-methylfuran and 3-methylfuran SOA are dominated by $C_{4\text{-}5}$ compounds with 7 to 8 oxygen atoms, whereas CHON species in furfural SOA are distributed over a wider range of carbon number and oxygen number, generally containing fewer than 5 oxygen atoms.

3.3 Volatility of furanoid SOA

The 2-D thermograms of furanoid SOA obtained from FIGAERO-CIMS are shown in Figure 4. These thermograms summarize the signal intensity of identified particle-phase compounds as a function of desorption temperature, allowing comparison of thermal desorption behavior across the examined furanoid SOA. Individual species in furfural SOA desorb across a much wider temperature window (~40 °C to 180 °C) compared to 2- and 3-methylfuran SOA, which shows a high-intensity signal band centered around ~80 °C. This trend is well reflected in the signal-weighted-average thermograms (red lines in Figure 4), where furfural SOA exhibits a higher T_{max} (144.5 °C) than 2- and 3-methylfuran SOA (T_{max} = 82.6 °C). The wide thermogram of furfural SOA arises from stronger signals in the lower-volatility bins (C* = $10^{-4.6}$ and $10^{-7.8}$ μg m^{-3}) compared to 2- and 3-methylfuran SOA. In addition to the higher T_{max}, the broader signal distribution of furfural SOA suggests a more diverse chemical composition with a wide range of volatility compared to methylfuran SOA. We note that the signal-weighted-average thermograms of all furanoid SOA in this study are broader and exhibit higher T_{max} values (82.6–144.5 °C) than those obtained during single-compound calibrations (e.g., glutaric acid, $C_5H_8O_4$, T_{max} = 43°C) (Joo et al., 2024a), suggesting the presence of oligomeric species in furanoid SOA in addition to C_5 monomers.

https://doi.org/10.5194/egusphere-2026-4881
Preprint. Discussion started: 19 August 2026

4 Discussion

4.1 Distinct radical chemistry of furfural among furanoids

The difference in temporal variations of NO and NO_2 between furfural (Figure 1a) and 2- and 3-methylfuran (Figure 1c and e) experiments indicates that the radical chemistry following furanoid+OH reaction can vary depending on the furanoid structure. The initial decrease in NO_2 and concurrent increase in NO at the onset of furfural photooxidation suggest that radicals such as alkyl radicals (R) can consume NO_2, which is converted into NO, instead of undergoing the typical RO_2+NO channel observed in the methylfuran experiments. We also note that there could be potential interference in the observed increase of NO from peroxyacylnitrate (PAN)-like species formed during acyl peroxy radical reaction pathways. Our results confirm previous theoretical studies that explored photooxidation of furfural and methylfuran isomers (Yuan et al., 2017; Zhao and Wang, 2017), and the oxidation mechanism is detailed in Figures 5 (simplified) and S4 (extended). Once photooxidation reactions are initiated by OH addition at the 2 or 5 position of substituted furanoids, which have lower energy barriers than OH addition at the 3 or 4 position, hydroxyalkyl radicals generated during furfural+OH (F-R1 and F-R2) preferentially react with NO_2 (or HO_2/RO_2, O_3) to form hydroxyalkoxyl radicals (F-AR1 and F-AR2) via R+NO_2 reaction channel (Figure 5a). Although a previous theoretical study suggested that the typically expected RO_2 (F-PR1) formation pathway can be favored under high NO conditions (Zhao and Wang, 2017), the elevated NO_2 levels in this study may have limited this pathway. This reaction channel can be followed by the decomposition pathway to form a heterocyclic hydroxy carbonyl (R(OH)(O), $C_4H_4O_3$) or an organic acid (R(O)COOH, $C_4H_4O_3$), which show the strongest signal intensity from HR-ToF-CIMS (Figure S2) and can compete with relatively minor reaction pathway that forms a ring-opened tricarbonyl compound, 4-oxo-2-pentendial ($C_5H_4O_3$). 4-oxo-2-pentendial is observed to form more rapidly than $C_4H_4O_3$ (Figure 1b). The effective first-order reaction constant for the formation of 4-oxo-2-pentendial is estimated to be ~2×10^4 s^{-1} via F-R3+O_2 reaction, whereas that for $C_4H_4O_3$ is estimated to be ~15 s^{-1} from F-R1/F-R2, assuming the rate constants of F-R1/F-R2 with NO_2 are similar to that of a simplified form of alkyl radical (i.e., CH_3 radical) reaction with NO_2 (Albaladejo et al., 2002; Zhao and Wang, 2017). Additionally, 4-oxo-2-pentendial can form via HO_2 abstraction of hydroxyperoxy radical (F-PR2), which is formed via ring-opened hydroxyalkyl radical

https://doi.org/10.5194/egusphere-2026-4881
Preprint. Discussion started: 19 August 2026

(F-R3) reaction with O_2. Unlike F-R1/R2, which are estimated to react slowly with O_2 compared to NO_2/HO_2/O_3, F-R3 reacts with O_2 sufficiently fast to form a peroxy radical (Zhao and Wang, 2017). Further reaction of 4-oxo-2-pentendial via H-abstraction by OH radical can generate dicarbonyl carboxylic acid (R(O)(O)COOH, $C_5H_4O_4$), which is identified as a major product in particle-phase mass spectra (Figure S3).

Because of the presence of aldehyde functionality, unlike 2- and 3-methylfuran, OH oxidation of furfural can proceed through an additional reaction channel besides the OH addition, which is an H-abstraction pathway to form an acyl peroxy radical (Zhao and Wang, 2017). Further reaction of F-PR3 with NO can lead to the formation of an organic acyl nitrate (R(O)ONO_2, $C_5H_3NO_5$), which shows the strongest signal among nitrogen-containing compounds in both gas and particle phases (Figure S2 and S3). Beyond the prominent gas-phase species shown in Figure S2, the F-PR3 reaction channel can additionally generate aged biomass burning plume markers such as maleic anhydride ($C_4H_2O_3$) and acyl peroxy nitrate ($C_5H_3NO_6$) (Figure 5a and S4a), which have been reported as fur-PAN (furoyl peroxynitrate) in previous studies (Coggon et al., 2019; Roberts et al., 2022).

Meanwhile, the hydroxyalkyl radicals (MF2-R1/R2, and MF3-R1/R2) formed from 2- and 3-methylfuran+OH reactions undergo O_2 addition to form hydroxyperoxy radicals (MF2-PR1/PR2 and MF3-PR1/PR2), which subsequently react with NO via RO_2+NO channel to produce cyclic hydroxyalkoxy radicals (MF2-AR1/AR2 and MF3-AR1/AR2). The alkoxy radicals subsequently decompose to form cyclic hydroxy carbonyl compounds ($C_5H_6O_3$ and $C_4H_4O_3$ from 2-methylfuran+OH, and $C_5H_6O_3$ from 3-methylfuran+OH reaction (Yuan et al., 2017)) (Figure 5b and c), which are identified as major oxidation products in Figure S2 and show a first-generation product temporal variation in Figure 1d and 1f. Similar to furfural, such reaction channel competes with the formation of dicarbonyl compounds such as 4-oxo-2-pentenal ($C_5H_6O_2$) and 2-methylbutenedial from 2-methylfuran+OH and 3-methylfuran+OH experiments, respectively. The ring-opening pathway is reported to be less favored, particularly for 3-methylfuran oxidation by OH radicals, compared to furfural or 2-methylfuran oxidation (Yuan et al., 2017; Aschmann et al., 2014). Still, these dicarbonyls are observed to form more rapidly compared to other first-generation products (Figure S5), as they are directly generated from alkyl radical (Figure S4b and c). Further reaction of these aldehydes via H-

https://doi.org/10.5194/egusphere-2026-4881
Preprint. Discussion started: 19 August 2026

abstraction by OH radicals can explain the formation of major gas-phase CHO species, including $C_5H_6O_3$ (a carbonyl carboxylic acid, Figure 5b and c), while also providing pathways to CHON species with prominent signals (Figure S2) such as organic acyl nitrate ($R(O)ONO_2$, $C_5H_5NO_5$). We note that carboxylic acids commonly found as major oxidation products in HR-ToF-CIMS measurements in this study can form via Baeyer−Villiger reaction during oligomerization processes (Claflin et al., 2018; Joo et al., 2019).

Gas-phase oxidation chemistry of the furanoids explored here shows that the substituent on the furan ring governs the radical pathways: $R+NO_2$ is more influential in furfural+OH reaction, whereas RO_2+NO chemistry dominates 2- and 3-methylfuran+OH reaction. Furthermore, even with the same substituent, different positional isomers (2- vs. 3-methylfuran) can divert the reaction channels, producing first-generation products with different carbon numbers (C_4 vs. C_5). This disparity in gas-phase oxidation across furanoid types drives differences in furanoid SOA formation potential and composition. Although ring-opening pathways are common for furanoids, $C_5H_6O_2$ and its subsequent oxidation products retain fewer oxygenated functional groups compared to the ring-opened first-generation product formed during the furfural+OH reaction ($C_5H_4O_3$), resulting in fewer reactive sites available for accretion reactions.

4.2 Oligomer formation and structural complexity of furfural SOA

Speciated SOA composition measured using FIGAERO-CIMS confirms the presence of oligomeric compounds in all furanoid SOA examined in this study. The relative abundances of compounds identified by FIGAERO-CIMS (Figure 3) demonstrate that dimeric species in the $C_{6\text{-}10}$ range comprise a sizable fraction of total detected particle-phase ion abundances (furfural SOA: 15% & 19%, 2-methylfuran SOA: 13% & 13%, 3-methylfuran SOA: 16% & 17% for CHO & CHON compounds, respectively). Additionally, the detected $C_{4\text{-}5}$ compounds include fragments produced by thermal decomposition of oligomers during the thermal desorption process in FIGAERO-CIMS. The presence of oligomers is further confirmed from offline LC-TOF filter analysis, which provides additional evidence for a range of C_{6+} accretion products, extending up to C_{32} (Figure S6). Furfural SOA appears to have a higher oligomer contribution with FIGAERO-CIMS thermogram and LC-TOF carbon

https://doi.org/10.5194/egusphere-2026-4881
Preprint. Discussion started: 19 August 2026

number distribution that extend substantially into higher molecular weight species (Figures 4 and S6). In addition to higher contributions from $C_{6\text{-}10}$ compounds, the fraction of $m/z > 50$ fragments detected by HR-ToF-AMS is also higher for furfural SOA compared to 2-methylfuran SOA and 3-methylfuran (Figure 2). Accordingly, this is consistent with the higher ΔM_o and SOA yield observed for furfural among all furanoids examined in this study (Table 1).

As proposed in Section 4.1, the greater availability of reactive sites for accretion reactions for molecules generated during photooxidation of furfural (Figure S4) suggests that the oxidation products can have molecular structures with more diverse functionalities. Furthermore, the broader high-signal band observed in the 2-D thermogram of furfural SOA (Figure 4) suggests the presence of more chemically diverse particle-phase products. Molecular information on furanoid SOA obtained from FIGAERO-CIMS (Figure 6) further indicates that furfural SOA has a lower but broader C* distribution and exhibits a higher average degree of unsaturation (DU = nC – (nH/2) + (nN/2) + 1) for a similar m/z range compared to 2- and 3-methylfuran SOA. It is well known that a higher level of DU can be associated with the presence of aromatics or oxygenated functionalities such as carbonyls and carboxylic acids, which may correspond to the higher fraction of $C_xH_yO_{z>1}$ species and a higher oxidation state (OSc = 2 × O:C – H:C) observed for furfural SOA (OSc = 1.32) compared to 2-methylfuran SOA (OSc = 1.19) and 3-methylfuran SOA (OSc = 0.60) in HR-ToF-AMS (Figure 2). An increase in the abundance of such functionalities can decrease volatility (Pankow and Asher, 2008), thereby facilitating SOA formation. Furthermore, the high DU of furfural SOA may be related to the stronger brown carbon formation reported previously (Joo et al., 2024a), as conjugated bonds that can increase DU are also known to enhance light-absorbing properties besides reduced CHON species that can be associated with amine, imine, or amide functional groups (Chen et al., 2022; Laskin et al., 2015).

4.3 Distinct CHON composition and organic nitrate formation in furanoid SOA

Differences in radical chemistry among furanoids (i.e., $R+NO_2$ and RO_2+NO pathways during furfural+OH and methylfuran+OH reactions, respectively) can distinctly influence the composition of CHON species in the particle phase. The products from these pathways differ; RO_2+NO reactions are known to generate alkoxy radicals (major pathway) and organic nitrate ($RONO_2$) (minor pathway)

https://doi.org/10.5194/egusphere-2026-4881
Preprint. Discussion started: 19 August 2026

(Perring et al., 2013), whereas R+NO_2 reaction can generate alkoxy radicals (major pathway) and nitro organics (RNO_2) (minor pathway) (Rissanen et al., 2010), which are generally more reduced than organic nitrate functionalities. Furthermore, furfural oxidation products can interact with NH_3/NH_4^+ at the particle surface to form reduced nitrogen functionalities such as amine or amide during photooxidation (Joo et al., 2024a). Results from FIGAERO-CIMS (Figure 3) demonstrate this difference, showing relatively predominant, less oxygenated CHON ($C_xH_yN_nO_{\leq 6}$) species across a wide range of carbon number in furfural SOA, whereas CHON species in 2- and 3-methylfuran SOA are relatively more oxygenated, with signal intensities concentrated at $C_{4\text{-}5}H_yN_nO_7$ compounds. When all the detected CHON species are lumped into two classes (O/N≥3 and O/N<3) (Figure 7), 19.0% of the furfural SOA signal measured by FIGAERO-CIMS is attributed to CHON species with higher O/N ratios (O/N≥3), whereas 8.3% is attributed to CHON species with lower O/N ratios (O/N<3). Compared to furfural SOA, CHON species with O/N≥3 contribute a larger fraction of the total FIGAERO-CIMS signal in 2-methylfuran and 3-methylfuran SOA, accounting for 35.1% and 24.2%, respectively, while CHON species with O/N<3 contribute 0.6% and 0.2%, respectively. The bulk composition analysis by LC-ESI-Q-ToF further supports these observations (Figure S7), showing a higher relative contribution of CHON species with O/N≥3 in 2- and 3-methylfuran SOA than in furfural SOA.

CHON species with O/N≥3 are likely associated with the formation of organic nitrate compounds, especially for species measured using FIGAERO-CIMS, considering their high sensitivity toward iodide reagent ion (Lee et al., 2014; Takeuchi and Ng, 2019). Accordingly, we estimate the particulate organic nitrate to organic aerosol ratio ($pRONO_2$/Org) using the method proposed by Takeuchi et al. (2024), which leverages R_{ON} (NO^+/NO_2^+ ratio of organic nitrate) and R_{AN} (NO^+/NO_2^+ ratio of ammonium nitrate) obtained from HR-ToF-AMS (Table S2), together with molecular weight of CHON (O/N≥3) species (furfural: 137.8 g mol^{-1} / 2-methylfuran: 191.3 g mol^{-1} / 3-methylfuran: 203.0 g mol^{-1}) obtained from FIGAERO-CIMS (Figure 7d). In this study, 2-methylfuran SOA shows the highest $pRONO_2$/Org ratio (45%), followed by 3-methylfuran SOA (36%), and furfural SOA (11%), consistent with the relative fraction of CHON species with O/N≥3 observed from both FIGAERO-CIMS and LC-ESI-Q-ToF measurements. It should also be noted that $pRONO_2$/Org values may be influenced by

https://doi.org/10.5194/egusphere-2026-4881
Preprint. Discussion started: 19 August 2026

fragmentation of other nitrogen-containing organics in HR-ToF-AMS measurements, particularly nitro compounds (Xu et al., 2021).

5 Conclusions and implications

This work investigates photooxidation chemistry and SOA formation from reactions of furanoids with OH radicals. Among the furanoids examined, furfural+OH reaction generates the highest SOA yield (9.8%) with a corresponding organic mass concentration of 66.3 μg m^{-3}, followed by SOA formed during 2-methylfuran+OH (1.2% at 8.9 μg m^{-3}) and 3-methylfuran+OH reaction (1.0% at 6.9 μg m^{-3}). A previous study reported that furanoids can contribute up to 51% of potential SOA depending on the type of fuel combusted (Hatch et al., 2015). Given the large emissions of furfural from various biomass burning fuels such as ponderosa pine and rice straw (Ciccioli et al., 2001; Gilman et al., 2015; Hatch et al., 2015), our findings suggest that furfural can be the most important SOA precursor among furanoids emitted from the biomass burning across different continents.

The difference in the amount of SOA formed can be closely associated with the molecular structure characteristics of furanoid SOA. Furfural SOA exhibits greater molecular complexity, with a lower but broader C* distribution and a higher average DU within a similar *m/z* range compared to 2- and 3-methylfuran SOA. The molecular complexity of furfural SOA can be relevant to multigenerational oxidation products generated from the first-generation ring-opened tricarbonyl ($C_5H_4O_3$), which retains more reactive sites available compared to oxidation products of dicarbonyls ($C_5H_6O_2$) generated during 2- and 3-methylfuran SOA formation. Even among alkyl-substituted furanoids, the distribution of first-generation oxidation products differs by isomer type. Methyl substitution at the 2-position yields both C_4 and C_5 products, whereas substitution at the 3-position predominantly yields C_5 products. These differences may have driven variations in SOA composition and volatility between methylfuran isomers.

While biomass burning is generally understood to enhance ozone formation (Jin et al.; Xu et al., 2022), large emissions of furfural during biomass burning can add complexity when detailed radical reactions are integrated to estimate ozone production. Unlike 2- and 3-methylfuran that undergo typical RO_2+NO reaction that produces NO_2, which can form ozone through subsequent photochemical reactions, furfural oxidation is influenced by the R+NO_2 channel. This radical reaction channel

https://doi.org/10.5194/egusphere-2026-4881
Preprint. Discussion started: 19 August 2026

consumes NO_2 and yields NO, which can titrate ozone. In addition, the alkyl radical from furfural+OH can directly consume ozone, competing with NO_2 to form alkoxy radical and bypassing the formation of peroxy radical (Zhao and Wang, 2017). Furthermore, compared to 2- and 3-methylfuran+OH reaction, furfural+OH reaction forms fewer organic nitrates, which can serve as NO_x reservoirs that can affect ozone formation downwind of the biomass burning plume (Alvarado et al., 2010).

Furanoids are often regarded as indicators of fresh biomass burning plumes, but their concentrations can decrease rapidly once released into the atmosphere owing to their high reactivity toward OH and NO_3 radicals. Accordingly, Müller et al. (2016) and Coggon et al. (2019) suggested that maleic anhydride ($C_4H_2O_3$) can serve as a tracer of aged biomass burning plumes far downwind of the source, since its lifetime can exceed 5 days at typical tropospheric OH concentration (1.5×10^6 molec. cm^{-3}). Additionally, Roberts et al. (2022) proposed fur-PAN ($C_5H_3NO_6$) as a photochemical biomass burning tracer, with an order of magnitude enhancement compared to urban background level when biomass burning plume hit Pasadena, CA. We identified these two compounds in the furfural+OH reaction, but only maleic anhydride exhibits a continuous increase throughout the experiment (Figure S5), suggesting that it is more representative of an aged biomass burning plume marker under the experimental conditions examined in this study. Furthermore, the presence of $C_4H_2O_3$ and its continuous increasing temporal trend are also observed in the 2-methylfuran+OH and 3-methylfuran+OH experiments, indicating that this compound may serve as a robust indicator of aged biomass burning influences associated with furanoid emissions.

Most current atmospheric models treat furanoids as a single compound class, and even those incorporating furanoid-specific reaction mechanisms often consider only alkyl-substituted variants while neglecting functionalized species (Romanias et al., 2024). The observed variability in gas phase photooxidation chemistry, SOA yield, and SOA composition across furanoid types implies that model parameterization and OH reactivity estimates should account for differences in functionalization. More importantly, our results suggest that substituent type can substantially influence radical chemistry, SOA formation, and SOA composition more strongly than isomeric differences among precursor furanoids. Thus, differentiating furfural from alkyl-substituted furanoids is important for improving our understanding of the chemical evolution of biomass burning plumes and their impacts on air quality.

https://doi.org/10.5194/egusphere-2026-4881
Preprint. Discussion started: 19 August 2026

Data Availability

The chamber experiment data reported in this study will be made available at the time of publication in the Index of Chamber Atmospheric Research in the United States (ICARUS) database.

Author contribution

TJ and NLN designed the environmental chamber experiments conducted in this study with inputs from MJA. TJ and DP performed chamber experiments, and TJ compiled and analyzed data obtained from all operated instruments. JEM, TH-M, and DRG analyzed offline filter data via LC-ESI-Q-ToF. JCR helped develop oxidation mechanisms. TJ and NLN prepared the original manuscript with contributions from all co-authors.

Competing interests

At least one of the (co-)authors is a member of the editorial board of *Atmospheric Chemistry and Physics*. The authors have no other competing interests to declare.

Acknowledgements

This research was supported by NSF AGS-1830727. The FIGAERO-CIMS was purchased through NSF Major Research Instrumentation (MRI) Grant 1428738. TJ additionally acknowledges National Research Foundation of Korea (NRF) grant funded by the Korea government (MSIT) (RS-2026-25471981) and Korea University Grant for the support. DRG, JEM, and TH-M would like to acknowledge NSF AGS-1764126. ChatGPT was used to assist in refining the grammar and clarity of the manuscript.

https://doi.org/10.5194/egusphere-2026-4881
Preprint. Discussion started: 19 August 2026

References

Abatzoglou, J. T. and Williams, A. P.: Impact of anthropogenic climate change on wildfire across western US forests, Proceedings of the National Academy of Sciences, 113, 11770–11775, 10.1073/pnas.1607171113, 2016.

Aiken, A. C., DeCarlo, P. F., and Jimenez, J. L.: Elemental Analysis of Organic Species with Electron Ionization High-Resolution Mass Spectrometry, Analytical Chemistry, 79, 8350–8358, 10.1021/ac071150w, 2007.

Akagi, S. K., Yokelson, R. J., Wiedinmyer, C., Alvarado, M. J., Reid, J. S., Karl, T., Crounse, J. D., and Wennberg, P. O.: Emission factors for open and domestic biomass burning for use in atmospheric models, Atmos. Chem. Phys., 11, 4039–4072, 10.5194/acp-11-4039-2011, 2011.

Akherati, A., He, Y., Coggon, M. M., Koss, A. R., Hodshire, A. L., Sekimoto, K., Warneke, C., de Gouw, J., Yee, L., Seinfeld, J. H., Onasch, T. B., Herndon, S. C., Knighton, W. B., Cappa, C. D., Kleeman, M. J., Lim, C. Y., Kroll, J. H., Pierce, J. R., and Jathar, S. H.: Oxygenated Aromatic Compounds are Important Precursors of Secondary Organic Aerosol in Biomass-Burning Emissions, Environmental Science & Technology, 54, 8568–8579, 10.1021/acs.est.0c01345, 2020.

Al Ali, F., Cœur, C., Houzel, N., Genevray, P., Cazier, F., Cuisset, A., Papadimitriou, V. C., Tomas, A., and Romanias, M. N.: Products and yields for the NO3 radical initiated atmospheric degradation of 2-methylfuran (2-MF, CH3–C4H3O), Atmospheric Environment, 319, 120276, https://doi.org/10.1016/j.atmosenv.2023.120276, 2024.

Albaladejo, J., Jiménez, E., Notario, A., Cabañas, B., and Martínez, E.: CH3O Yield in the CH3 + O3 Reaction Using the LP/LIF Technique at Room Temperature, The Journal of Physical Chemistry A, 106, 2512–2519, 10.1021/jp012249o, 2002.

Alfarra, M. R., Coe, H., Allan, J. D., Bower, K. N., Boudries, H., Canagaratna, M. R., Jimenez, J. L., Jayne, J. T., Garforth, A. A., Li, S.-M., and Worsnop, D. R.: Characterization of urban and rural organic particulate in the Lower Fraser Valley using two Aerodyne Aerosol Mass Spectrometers, Atmospheric Environment, 38, 5745–5758, https://doi.org/10.1016/j.atmosenv.2004.01.054, 2004.

Aljawhary, D., Lee, A. K. Y., and Abbatt, J. P. D.: High-resolution chemical ionization mass spectrometry (ToF-CIMS): application to study SOA composition and processing, Atmos. Meas. Tech., 6, 3211–3224, 10.5194/amt-6-3211-2013, 2013.

Alvarado, M. J. and Prinn, R. G.: Formation of ozone and growth of aerosols in young smoke plumes from biomass burning: 1. Lagrangian parcel studies, Journal of Geophysical Research: Atmospheres, 114, https://doi.org/10.1029/2008JD011144, 2009.

Alvarado, M. J., Lonsdale, C. R., Yokelson, R. J., Akagi, S. K., Coe, H., Craven, J. S., Fischer, E. V., McMeeking, G. R., Seinfeld, J. H., Soni, T., Taylor, J. W., Weise, D. R., and Wold, C. E.: Investigating the links between ozone and organic aerosol chemistry in a biomass burning plume from a prescribed fire in California chaparral, Atmos. Chem. Phys., 15, 6667–6688, 10.5194/acp-15-6667-2015, 2015.

Alvarado, M. J., Logan, J. A., Mao, J., Apel, E., Riemer, D., Blake, D., Cohen, R. C., Min, K. E., Perring, A. E., Browne, E. C., Wooldridge, P. J., Diskin, G. S., Sachse, G. W., Fuelberg, H., Sessions, W. R., Harrigan, D. L., Huey, G., Liao, J., Case-Hanks, A., Jimenez, J. L., Cubison, M. J., Vay, S. A., Weinheimer, A. J., Knapp, D. J., Montzka, D. D., Flocke, F. M., Pollack, I. B., Wennberg, P. O., Kurten, A., Crounse, J., Clair, J. M. S., Wisthaler, A., Mikoviny, T., Yantosca, R. M., Carouge, C. C., and Le Sager, P.: Nitrogen oxides and PAN in plumes from boreal fires during ARCTAS-B and their impact on ozone: an integrated analysis of aircraft and satellite observations, Atmos. Chem. Phys., 10, 9739–9760, 10.5194/acp-10-9739-2010, 2010.

Aschmann, S. M., Nishino, N., Arey, J., and Atkinson, R.: Kinetics of the Reactions of OH Radicals with 2- and 3-Methylfuran, 2,3- and 2,5-Dimethylfuran, and E- and Z-3-Hexene-2,5-dione, and Products of OH + 2,5-Dimethylfuran, Environmental Science & Technology, 45, 1859–1865, 10.1021/es103207k, 2011.

Aschmann, S. M., Nishino, N., Arey, J., and Atkinson, R.: Products of the OH Radical-Initiated Reactions of Furan, 2- and 3-Methylfuran, and 2,3- and 2,5-Dimethylfuran in the Presence of NO, The Journal of Physical Chemistry A, 118, 457–466, 10.1021/jp410345k, 2014.

Bahreini, R., Keywood, M. D., Ng, N. L., Varutbangkul, V., Gao, S., Flagan, R. C., Seinfeld, J. H., Worsnop, D. R., and Jimenez, J. L.: Measurements of Secondary Organic Aerosol from Oxidation of Cycloalkenes, Terpenes, and m-Xylene Using an Aerodyne Aerosol Mass Spectrometer, Environmental Science & Technology, 39, 5674–5688, 10.1021/es048061a, 2005.

https://doi.org/10.5194/egusphere-2026-4881
Preprint. Discussion started: 19 August 2026

Bierbach, A., Barnes, I., and Becker, K. H.: Product and kinetic study of the oh-initiated gas-phase oxidation of Furan, 2-methylfuran and furanaldehydes at ≈ 300 K, Atmospheric Environment, 29, 2651–2660, https://doi.org/10.1016/1352-2310(95)00096-H, 1995.

Boyd, C. M., Sanchez, J., Xu, L., Eugene, A. J., Nah, T., Tuet, W. Y., Guzman, M. I., and Ng, N. L.: Secondary organic aerosol formation from the β-pinene+NO₃ system: effect of humidity and peroxy radical fate, Atmos. Chem. Phys., 15, 7497–7522, 10.5194/acp-15-7497-2015, 2015.

Bruns, E. A., El Haddad, I., Slowik, J. G., Kilic, D., Klein, F., Baltensperger, U., and Prévôt, A. S. H.: Identification of significant precursor gases of secondary organic aerosols from residential wood combustion, Scientific Reports, 6, 27881, 10.1038/srep27881, 2016.

Burke, M., Childs, M. L., de la Cuesta, B., Qiu, M., Li, J., Gould, C. F., Heft-Neal, S., and Wara, M.: The contribution of wildfire to PM2.5 trends in the USA, Nature, 622, 761–766, 10.1038/s41586-023-06522-6, 2023.

Canagaratna, M. R., Jimenez, J. L., Kroll, J. H., Chen, Q., Kessler, S. H., Massoli, P., Hildebrandt Ruiz, L., Fortner, E., Williams, L. R., Wilson, K. R., Surratt, J. D., Donahue, N. M., Jayne, J. T., and Worsnop, D. R.: Elemental ratio measurements of organic compounds using aerosol mass spectrometry: characterization, improved calibration, and implications, Atmos. Chem. Phys., 15, 253–272, 10.5194/acp-15-253-2015, 2015.

Chen, K., Raeofy, N., Lum, M., Mayorga, R., Woods, M., Bahreini, R., Zhang, H., and Lin, Y.-H.: Solvent effects on chemical composition and optical properties of extracted secondary brown carbon constituents, Aerosol Science and Technology, 56, 917–930, 10.1080/02786826.2022.2100734, 2022.

Ciccioli, P., Brancaleoni, E., Frattoni, M., Cecinato, A., and Pinciarelli, L.: DETERMINATION OF VOLATILE ORGANIC COMPOUNDS (VOC) EMITTED FROM BIOMASS BURNING OF MEDITERRANEAN VEGETATION SPECIES BY GC-MS, Analytical Letters, 34, 937–955, 10.1081/AL-100103604, 2001.

Claflin, M. S., Krechmer, J. E., Hu, W., Jimenez, J. L., and Ziemann, P. J.: Functional Group Composition of Secondary Organic Aerosol Formed from Ozonolysis of α-Pinene Under High VOC and Autoxidation Conditions, ACS Earth and Space Chemistry, 2, 1196–1210, 10.1021/acsearthspacechem.8b00117, 2018.

Coggon, M. M., Lim, C. Y., Koss, A. R., Sekimoto, K., Yuan, B., Gilman, J. B., Hagan, D. H., Selimovic, V., Zarzana, K. J., Brown, S. S., Roberts, J. M., Müller, M., Yokelson, R., Wisthaler, A., Krechmer, J. E., Jimenez, J. L., Cappa, C., Kroll, J. H., de Gouw, J., and Warneke, C.: OH chemistry of non-methane organic gases (NMOGs) emitted from laboratory and ambient biomass burning smoke: evaluating the influence of furans and oxygenated aromatics on ozone and secondary NMOG formation, Atmos. Chem. Phys., 19, 14875–14899, 10.5194/acp-19-14875-2019, 2019.

Colmenar, I., Martín, P., Cabañas, B., Salgado, S., Villanueva, F., and Ballesteros, B.: Evaluation of the SOA Formation in the Reaction of Furfural with Atmospheric Oxidants, Atmosphere, 11, 927, 2020.

Crutzen, P. J. and Andreae, M. O.: Biomass Burning in the Tropics: Impact on Atmospheric Chemistry and Biogeochemical Cycles, Science, 250, 1669–1678, 10.1126/science.250.4988.1669, 1990.

Daellenbach, K. R., Uzu, G., Jiang, J., Cassagnes, L.-E., Leni, Z., Vlachou, A., Stefenelli, G., Canonaco, F., Weber, S., Segers, A., Kuenen, J. J. P., Schaap, M., Favez, O., Albinet, A., Aksoyoglu, S., Dommen, J., Baltensperger, U., Geiser, M., El Haddad, I., Jaffrezo, J.-L., and Prévôt, A. S. H.: Sources of particulate-matter air pollution and its oxidative potential in Europe, Nature, 587, 414–419, 10.1038/s41586-020-2902-8, 2020.

DeCarlo, P. F., Kimmel, J. R., Trimborn, A., Northway, M. J., Jayne, J. T., Aiken, A. C., Gonin, M., Fuhrer, K., Horvath, T., Docherty, K. S., Worsnop, D. R., and Jimenez, J. L.: Field-Deployable, High-Resolution, Time-of-Flight Aerosol Mass Spectrometer, Analytical Chemistry, 78, 8281–8289, 10.1021/ac061249n, 2006.

Decker, Z. C. J., Zarzana, K. J., Coggon, M., Min, K.-E., Pollack, I., Ryerson, T. B., Peischl, J., Edwards, P., Dubé, W. P., Markovic, M. Z., Roberts, J. M., Veres, P. R., Graus, M., Warneke, C., de Gouw, J., Hatch, L. E., Barsanti, K. C., and Brown, S. S.: Nighttime Chemical Transformation in Biomass Burning Plumes: A Box Model Analysis Initialized with Aircraft Observations, Environmental Science & Technology, 53, 2529–2538, 10.1021/acs.est.8b05359, 2019.

Decker, Z. C. J., Robinson, M. A., Barsanti, K. C., Bourgeois, I., Coggon, M. M., DiGangi, J. P., Diskin, G. S., Flocke, F. M., Franchin, A., Fredrickson, C. D., Gkatzelis, G. I., Hall, S. R., Halliday, H., Holmes, C. D., Huey, L. G., Lee, Y. R., Lindaas, J., Middlebrook, A. M., Montzka, D. D., Moore, R., Neuman, J. A., Nowak, J. B., Palm, B. B., Peischl, J., Piel, F., Rickly, P. S., Rollins, A. W., Ryerson, T. B., Schwantes, R. H., Sekimoto, K., Thornhill, L., Thornton, J. A., Tyndall, G. S., Ullmann, K., Van Rooy, P., Veres, P. R., Warneke, C., Washenfelder, R. A., Weinheimer, A. J., Wiggins, E., Winstead, E., Wisthaler, A., Womack, C., and Brown, S. S.: Nighttime and daytime dark oxidation

https://doi.org/10.5194/egusphere-2026-4881
Preprint. Discussion started: 19 August 2026

chemistry in wildfire plumes: an observation and model analysis of FIREX-AQ aircraft data, Atmos. Chem. Phys., 21, 16293–16317, 10.5194/acp-21-16293-2021, 2021.

Ditto, J. C., Barnes, E. B., Khare, P., Takeuchi, M., Joo, T., Bui, A. A. T., Lee-Taylor, J., Eris, G., Chen, Y., Aumont, B., Jimenez, J. L., Ng, N. L., Griffin, R. J., and Gentner, D. R.: An omnipresent diversity and variability in the chemical composition of atmospheric functionalized organic aerosol, Communications Chemistry, 1, 75, 10.1038/s42004-018-0074-3, 2018.

Fang, Z., Deng, W., Zhang, Y., Ding, X., Tang, M., Liu, T., Hu, Q., Zhu, M., Wang, Z., Yang, W., Huang, Z., Song, W., Bi, X., Chen, J., Sun, Y., George, C., and Wang, X.: Open burning of rice, corn and wheat straws: primary emissions, photochemical aging, and secondary organic aerosol formation, Atmos. Chem. Phys., 17, 14821–14839, 10.5194/acp-17-14821-2017, 2017.

Gilman, J. B., Lerner, B. M., Kuster, W. C., Goldan, P. D., Warneke, C., Veres, P. R., Roberts, J. M., de Gouw, J. A., Burling, I. R., and Yokelson, R. J.: Biomass burning emissions and potential air quality impacts of volatile organic compounds and other trace gases from fuels common in the US, Atmos. Chem. Phys., 15, 13915–13938, 10.5194/acp-15-13915-2015, 2015.

Gómez Alvarez, E., Borrás, E., Viidanoja, J., and Hjorth, J.: Unsaturated dicarbonyl products from the OH-initiated photo-oxidation of furan, 2-methylfuran and 3-methylfuran, Atmospheric Environment, 43, 1603–1612, 10.1016/j.atmosenv.2008.12.019, 2009.

Grieshop, A. P., Logue, J. M., Donahue, N. M., and Robinson, A. L.: Laboratory investigation of photochemical oxidation of organic aerosol from wood fires 1: measurement and simulation of organic aerosol evolution, Atmos. Chem. Phys., 9, 1263–1277, 10.5194/acp-9-1263-2009, 2009.

Hatch, L. E., Luo, W., Pankow, J. F., Yokelson, R. J., Stockwell, C. E., and Barsanti, K. C.: Identification and quantification of gaseous organic compounds emitted from biomass burning using two-dimensional gas chromatography–time-of-flight mass spectrometry, Atmos. Chem. Phys., 15, 1865–1899, 10.5194/acp-15-1865-2015, 2015.

Hatch, L. E., Yokelson, R. J., Stockwell, C. E., Veres, P. R., Simpson, I. J., Blake, D. R., Orlando, J. J., and Barsanti, K. C.: Multi-instrument comparison and compilation of non-methane organic gas emissions from biomass burning and implications for smoke-derived secondary organic aerosol precursors, Atmos. Chem. Phys., 17, 1471–1489, 10.5194/acp-17-1471-2017, 2017.

Jen, C. N., Hatch, L. E., Selimovic, V., Yokelson, R. J., Weber, R., Fernandez, A. E., Kreisberg, N. M., Barsanti, K. C., and Goldstein, A. H.: Speciated and total emission factors of particulate organics from burning western US wildland fuels and their dependence on combustion efficiency, Atmos. Chem. Phys., 19, 1013–1026, 10.5194/acp-19-1013-2019, 2019.

Jiang, J., Carter, W. P. L., Cocker, D. R., and Barsanti, K. C.: Development and Evaluation of a Detailed Mechanism for Gas-Phase Atmospheric Reactions of Furans, ACS Earth and Space Chemistry, 4, 1254–1268, 10.1021/acsearthspacechem.0c00058, 2020.

Jiang, X., Tsona, N. T., Jia, L., Liu, S., Zhang, H., Xu, Y., and Du, L.: Secondary organic aerosol formation from photooxidation of furan: effects of NOx and humidity, Atmos. Chem. Phys., 19, 13591–13609, 10.5194/acp-19-13591-2019, 2019.

Jin, L., Coggon, M. M., Permar, W., Juncosa Calahorrano, J. F., Palm, B. B., Gkatzelis, G. I., Robinson, M. A., Bourgeois, I., Hall, S. R., Peischl, J., Ullmann, K., Thornton, J. A., Warneke, C., Flocke, F., Fischer, E. V., Yokelson, R. J., and Hu, L.: Ozone photochemistry in fresh biomass burning smoke over the United States, Science Advances, 12, eads2157, 10.1126/sciadv.ads2157,

Joo, T., Rivera-Rios, J. C., Takeuchi, M., Alvarado, M. J., and Ng, N. L.: Secondary Organic Aerosol Formation from Reaction of 3-Methylfuran with Nitrate Radicals, ACS Earth and Space Chemistry, 3, 922–934, 10.1021/acsearthspacechem.9b00068, 2019.

Joo, T., Machesky, J. E., Zeng, L., Hass-Mitchell, T., Weber, R. J., Gentner, D. R., and Ng, N. L.: Secondary Brown Carbon Formation From Photooxidation of Furans From Biomass Burning, Geophysical Research Letters, 51, e2023GL104900, https://doi.org/10.1029/2023GL104900, 2024a.

Joo, T., Rogers, M. J., Soong, C., Hass-Mitchell, T., Heo, S., Bell, M. L., Ng, N. L., and Gentner, D. R.: Aged and Obscured Wildfire Smoke Associated with Downwind Health Risks, Environmental Science & Technology Letters, 11, 1340–1347, 10.1021/acs.estlett.4c00785, 2024b.

https://doi.org/10.5194/egusphere-2026-4881
Preprint. Discussion started: 19 August 2026

Koss, A. R., Sekimoto, K., Gilman, J. B., Selimovic, V., Coggon, M. M., Zarzana, K. J., Yuan, B., Lerner, B. M., Brown, S. S., Jimenez, J. L., Krechmer, J., Roberts, J. M., Warneke, C., Yokelson, R. J., and de Gouw, J.: Non-methane organic gas emissions from biomass burning: identification, quantification, and emission factors from PTR-ToF during the FIREX 2016 laboratory experiment, Atmos. Chem. Phys., 18, 3299–3319, 10.5194/acp-18-3299-2018, 2018.

Kroll, J. H. and Seinfeld, J. H.: Chemistry of secondary organic aerosol: Formation and evolution of low-volatility organics in the atmosphere, Atmospheric Environment, 42, 3593–3624, 2008.

Laskin, A., Laskin, J., and Nizkorodov, S. A.: Chemistry of Atmospheric Brown Carbon, Chemical Reviews, 115, 4335–4382, 10.1021/cr5006167, 2015.

Lee, B. H., Lopez-Hilfiker, F. D., Mohr, C., Kurtén, T., Worsnop, D. R., and Thornton, J. A.: An Iodide-Adduct High-Resolution Time-of-Flight Chemical-Ionization Mass Spectrometer: Application to Atmospheric Inorganic and Organic Compounds, Environmental Science & Technology, 48, 6309–6317, 10.1021/es500362a, 2014.

Lim, C. Y., Hagan, D. H., Coggon, M. M., Koss, A. R., Sekimoto, K., de Gouw, J., Warneke, C., Cappa, C. D., and Kroll, J. H.: Secondary organic aerosol formation from the laboratory oxidation of biomass burning emissions, Atmos. Chem. Phys., 19, 12797–12809, 10.5194/acp-19-12797-2019, 2019.

Liu, F., Joo, T., Ditto, J. C., Saavedra, M. G., Takeuchi, M., Boris, A. J., Yang, Y., Weber, R. J., Dillner, A. M., Gentner, D. R., and Ng, N. L.: Oxidized and Unsaturated: Key Organic Aerosol Traits Associated with Cellular Reactive Oxygen Species Production in the Southeastern United States, Environmental Science & Technology, 57, 14150–14161, 10.1021/acs.est.3c03641, 2023.

Lopez-Hilfiker, F. D., Mohr, C., Ehn, M., Rubach, F., Kleist, E., Wildt, J., Mentel, T. F., Lutz, A., Hallquist, M., Worsnop, D., and Thornton, J. A.: A novel method for online analysis of gas and particle composition: description and evaluation of a Filter Inlet for Gases and AEROsols (FIGAERO), Atmos. Meas. Tech., 7, 983–1001, 10.5194/amt-7-983-2014, 2014.

Mettler, M. S., Mushrif, S. H., Paulsen, A. D., Javadekar, A. D., Vlachos, D. G., and Dauenhauer, P. J.: Revealing pyrolysis chemistry for biofuels production: Conversion of cellulose to furans and small oxygenates, Energy & Environmental Science, 5, 5414–5424, 10.1039/C1EE02743C, 2012.

Müller, M., Anderson, B. E., Beyersdorf, A. J., Crawford, J. H., Diskin, G. S., Eichler, P., Fried, A., Keutsch, F. N., Mikoviny, T., Thornhill, K. L., Walega, J. G., Weinheimer, A. J., Yang, M., Yokelson, R. J., and Wisthaler, A.: In situ measurements and modeling of reactive trace gases in a small biomass burning plume, Atmos. Chem. Phys., 16, 3813–3824, 10.5194/acp-16-3813-2016, 2016.

Nah, T., Sanchez, J., Boyd, C. M., and Ng, N. L.: Photochemical Aging of α-pinene and β-pinene Secondary Organic Aerosol formed from Nitrate Radical Oxidation, Environmental Science & Technology, 50, 222–231, 10.1021/acs.est.5b04594, 2016a.

Nah, T., McVay, R. C., Zhang, X., Boyd, C. M., Seinfeld, J. H., and Ng, N. L.: Influence of seed aerosol surface area and oxidation rate on vapor wall deposition and SOA mass yields: a case study with α-pinene ozonolysis, Atmos. Chem. Phys., 16, 9361–9379, 10.5194/acp-16-9361-2016, 2016b.

Ng, N. L., Canagaratna, M. R., Jimenez, J. L., Chhabra, P. S., Seinfeld, J. H., and Worsnop, D. R.: Changes in organic aerosol composition with aging inferred from aerosol mass spectra, Atmos. Chem. Phys., 11, 6465–6474, 10.5194/acp-11-6465-2011, 2011.

Palm, B. B., Peng, Q., Fredrickson, C. D., Lee, B. H., Garofalo, L. A., Pothier, M. A., Kreidenweis, S. M., Farmer, D. K., Pokhrel, R. P., Shen, Y., Murphy, S. M., Permar, W., Hu, L., Campos, T. L., Hall, S. R., Ullmann, K., Zhang, X., Flocke, F., Fischer, E. V., and Thornton, J. A.: Quantification of organic aerosol and brown carbon evolution in fresh wildfire plumes, Proceedings of the National Academy of Sciences, 202012218, 10.1073/pnas.2012218117, 2020.

Pankow, J. F. and Asher, W. E.: SIMPOL.1: a simple group contribution method for predicting vapor pressures and enthalpies of vaporization of multifunctional organic compounds, Atmos. Chem. Phys., 8, 2773–2796, 10.5194/acp-8-2773-2008, 2008.

Pardo, M., Li, C., Zimmermann, R., and Rudich, Y.: Health impacts of biomass burning aerosols: Relation to oxidative stress and inflammation, Aerosol Science and Technology, 58, 1093–1113, 10.1080/02786826.2024.2379551, 2024.

Peng, Q., Palm, B. B., Melander, K. E., Lee, B. H., Hall, S. R., Ullmann, K., Campos, T., Weinheimer, A. J., Apel, E. C., Hornbrook, R. S., Hills, A. J., Montzka, D. D., Flocke, F., Hu, L., Permar, W., Wielgasz, C., Lindaas, J., Pollack, I. B., Fischer, E. V., Bertram, T. H., and Thornton, J. A.: HONO Emissions from Western U.S. Wildfires Provide

https://doi.org/10.5194/egusphere-2026-4881
Preprint. Discussion started: 19 August 2026

Dominant Radical Source in Fresh Wildfire Smoke, Environmental Science & Technology, 54, 5954–5963, 10.1021/acs.est.0c00126, 2020.

Perring, A. E., Pusede, S. E., and Cohen, R. C.: An Observational Perspective on the Atmospheric Impacts of Alkyl and Multifunctional Nitrates on Ozone and Secondary Organic Aerosol, Chemical Reviews, 113, 5848–5870, 10.1021/cr300520x, 2013.

Pye, H. O. T., Ward-Caviness, C. K., Murphy, B. N., Appel, K. W., and Seltzer, K. M.: Secondary organic aerosol association with cardiorespiratory disease mortality in the United States, Nature Communications, 12, 7215, 10.1038/s41467-021-27484-1, 2021.

Reddington, C. L., Spracklen, D. V., Artaxo, P., Ridley, D. A., Rizzo, L. V., and Arana, A.: Analysis of particulate emissions from tropical biomass burning using a global aerosol model and long-term surface observations, Atmos. Chem. Phys., 16, 11083–11106, 10.5194/acp-16-11083-2016, 2016.

Rissanen, M. P., Arppe, S. L., Eskola, A. J., Tammi, M. M., and Timonen, R. S.: Kinetics of the R + NO2 Reactions (R = i-C3H7, n-C3H7, s-C4H9, and t-C4H9) in the Temperature Range 201−489 K, The Journal of Physical Chemistry A, 114, 4811–4817, 10.1021/jp909396v, 2010.

Roberts, J. M., Neuman, J. A., Brown, S. S., Veres, P. R., Coggon, M. M., Stockwell, C. E., Warneke, C., Peischl, J., and Robinson, M. A.: Furoyl peroxynitrate (fur-PAN), a product of VOC–NOx photochemistry from biomass burning emissions: photochemical synthesis, calibration, chemical characterization, and first atmospheric observations, Environmental Science: Atmospheres, 2, 1087–1100, 10.1039/D2EA00068G, 2022.

Romanias, M. N., Coggon, M. M., Al Ali, F., Burkholder, J. B., Dagaut, P., Decker, Z., Warneke, C., Stockwell, C. E., Roberts, J. M., Tomas, A., Houzel, N., Coeur, C., and Brown, S. S.: Emissions and Atmospheric Chemistry of Furanoids from Biomass Burning: Insights from Laboratory to Atmospheric Observations, ACS Earth and Space Chemistry, 8, 857–899, 10.1021/acsearthspacechem.3c00226, 2024.

Schueneman, M. K., Day, D. A., Peng, Z., Pagonis, D., Jenks, O. J., de Gouw, J. A., and Jimenez, J. L.: Secondary Organic Aerosol Formation from the OH Oxidation of Phenol, Catechol, Styrene, Furfural, and Methyl Furfural, ACS Earth and Space Chemistry, 8, 1179–1192, 10.1021/acsearthspacechem.3c00361, 2024.

Stark, H., Yatavelli, R. L. N., Thompson, S. L., Kang, H., Krechmer, J. E., Kimmel, J. R., Palm, B. B., Hu, W., Hayes, P. L., Day, D. A., Campuzano-Jost, P., Canagaratna, M. R., Jayne, J. T., Worsnop, D. R., and Jimenez, J. L.: Impact of Thermal Decomposition on Thermal Desorption Instruments: Advantage of Thermogram Analysis for Quantifying Volatility Distributions of Organic Species, Environmental Science & Technology, 51, 8491–8500, 10.1021/acs.est.7b00160, 2017.

Stefenelli, G., Jiang, J., Bertrand, A., Bruns, E. A., Pieber, S. M., Baltensperger, U., Marchand, N., Aksoyoglu, S., Prévôt, A. S. H., Slowik, J. G., and El Haddad, I.: Secondary organic aerosol formation from smoldering and flaming combustion of biomass: a box model parametrization based on volatility basis set, Atmos. Chem. Phys., 19, 11461–11484, 10.5194/acp-19-11461-2019, 2019.

Stockwell, C. E., Veres, P. R., Williams, J., and Yokelson, R. J.: Characterization of biomass burning emissions from cooking fires, peat, crop residue, and other fuels with high-resolution proton-transfer-reaction time-of-flight mass spectrometry, Atmos. Chem. Phys., 15, 845–865, 10.5194/acp-15-845-2015, 2015.

Strollo, C. M. and Ziemann, P. J.: Products and mechanism of secondary organic aerosol formation from the reaction of 3-methylfuran with OH radicals in the presence of NOx, Atmospheric Environment, 77, 534–543, https://doi.org/10.1016/j.atmosenv.2013.05.033, 2013.

Tajuelo, M., Rodríguez, D., Rodríguez, A., Escalona, A., Viteri, G., Aranda, A., and Diaz-de-Mera, Y.: Secondary organic aerosol formation from the ozonolysis and oh-photooxidation of 2,5-dimethylfuran, Atmospheric Environment, 245, 118041, https://doi.org/10.1016/j.atmosenv.2020.118041, 2021.

Takeuchi, M. and Ng, N. L.: Chemical composition and hydrolysis of organic nitrate aerosol formed from hydroxyl and nitrate radical oxidation of α-pinene and β-pinene, Atmos. Chem. Phys., 19, 12749–12766, 10.5194/acp-19-12749-2019, 2019.

Takeuchi, M., Wang, Y., Nault, B. A., Chen, Y., Canagaratna, M. R., and Ng, N. L.: Evaluating the response of the Aerodyne aerosol mass spectrometer to monoterpene- and isoprene-derived organic nitrate standards, Aerosol Science and Technology, 58, 1371–1388, 10.1080/02786826.2024.2389183, 2024.

Tapia, A., Villanueva, F., Salgado, M. S., Cabañas, B., Martínez, E., and Martín, P.: Atmospheric degradation of 3-methylfuran: kinetic and products study, Atmos. Chem. Phys., 11, 3227–3241, 10.5194/acp-11-3227-2011, 2011.

https://doi.org/10.5194/egusphere-2026-4881
Preprint. Discussion started: 19 August 2026

729 Tuet, W. Y., Chen, Y., Fok, S., Champion, J. A., and Ng, N. L.: Inflammatory responses to secondary organic aerosols (SOA)
730 generated from biogenic and anthropogenic precursors, Atmos. Chem. Phys., 17, 11423–11440, 10.5194/acp-17-
731 11423-2017, 2017.
732 Wang, D. S. and Hildebrandt Ruiz, L.: Chlorine-initiated oxidation of n-alkanes under high-NOx conditions: insights into
733 secondary organic aerosol composition and volatility using a FIGAERO–CIMS, Atmos. Chem. Phys., 18, 15535–
734 15553, 10.5194/acp-18-15535-2018, 2018.
735 Xu, L., Crounse John, D., Vasquez Krystal, T., Allen, H., Wennberg Paul, O., Bourgeois, I., Brown Steven, S., Campuzano-
736 Jost, P., Coggon Matthew, M., Crawford James, H., DiGangi Joshua, P., Diskin Glenn, S., Fried, A., Gargulinski
737 Emily, M., Gilman Jessica, B., Gkatzelis Georgios, I., Guo, H., Hair Johnathan, W., Hall Samuel, R., Halliday
738 Hannah, A., Hanisco Thomas, F., Hannun Reem, A., Holmes Christopher, D., Huey, L. G., Jimenez Jose, L.,
739 Lamplugh, A., Lee Young, R., Liao, J., Lindaas, J., Neuman, J. A., Nowak John, B., Peischl, J., Peterson David, A.,
740 Piel, F., Richter, D., Rickly Pamela, S., Robinson Michael, A., Rollins Andrew, W., Ryerson Thomas, B., Sekimoto,
741 K., Selimovic, V., Shingler, T., Soja Amber, J., St. Clair Jason, M., Tanner David, J., Ullmann, K., Veres Patrick,
742 R., Walega, J., Warneke, C., Washenfelder Rebecca, A., Weibring, P., Wisthaler, A., Wolfe Glenn, M., Womack
743 Caroline, C., and Yokelson Robert, J.: Ozone chemistry in western U.S. wildfire plumes, Science Advances, 7,
744 eabl3648, 10.1126/sciadv.abl3648, 2022.
745 Xu, W., Takeuchi, M., Chen, C., Qiu, Y., Xie, C., Xu, W., Ma, N., Worsnop, D. R., Ng, N. L., and Sun, Y.: Estimation of
746 particulate organic nitrates from thermodenuder–aerosol mass spectrometer measurements in the North China Plain,
747 Atmos. Meas. Tech., 14, 3693–3705, 10.5194/amt-14-3693-2021, 2021.
748 Yuan, Y., Zhao, X., Wang, S., and Wang, L.: Atmospheric Oxidation of Furan and Methyl-Substituted Furans Initiated by
749 Hydroxyl Radicals, The Journal of Physical Chemistry A, 121, 9306–9319, 10.1021/acs.jpca.7b09741, 2017.
750 Zhang, X., Cappa, C. D., Jathar, S. H., McVay, R. C., Ensberg, J. J., Kleeman, M. J., and Seinfeld, J. H.: Influence of vapor
751 wall loss in laboratory chambers on yields of secondary organic aerosol, Proceedings of the National Academy of
752 Sciences, 111, 5802–5807, 10.1073/pnas.1404727111, 2014.
753 Zhao, X. and Wang, L.: Atmospheric Oxidation Mechanism of Furfural Initiated by Hydroxyl Radicals, The Journal of
754 Physical Chemistry A, 121, 3247–3253, 10.1021/acs.jpca.7b00506, 2017.
755 Zhou, J., Elser, M., Huang, R. J., Krapf, M., Fröhlich, R., Bhattu, D., Stefenelli, G., Zotter, P., Bruns, E. A., Pieber, S. M., Ni,
756 H., Wang, Q., Wang, Y., Zhou, Y., Chen, C., Xiao, M., Slowik, J. G., Brown, S., Cassagnes, L. E., Daellenbach, K.
757 R., Nussbaumer, T., Geiser, M., Prévôt, A. S. H., El-Haddad, I., Cao, J., Baltensperger, U., and Dommen, J.:
758 Predominance of secondary organic aerosol to particle-bound reactive oxygen species activity in fine ambient
759 aerosol, Atmos. Chem. Phys., 19, 14703–14720, 10.5194/acp-19-14703-2019, 2019.
760 Ziemann, P. J. and Atkinson, R.: Kinetics, products, and mechanisms of secondary organic aerosol formation, Chemical
761 Society Reviews, 41, 6582–6605, 10.1039/C2CS35122F, 2012.
762

763

https://doi.org/10.5194/egusphere-2026-4881
Preprint. Discussion started: 19 August 2026

764 **Figures and Table**

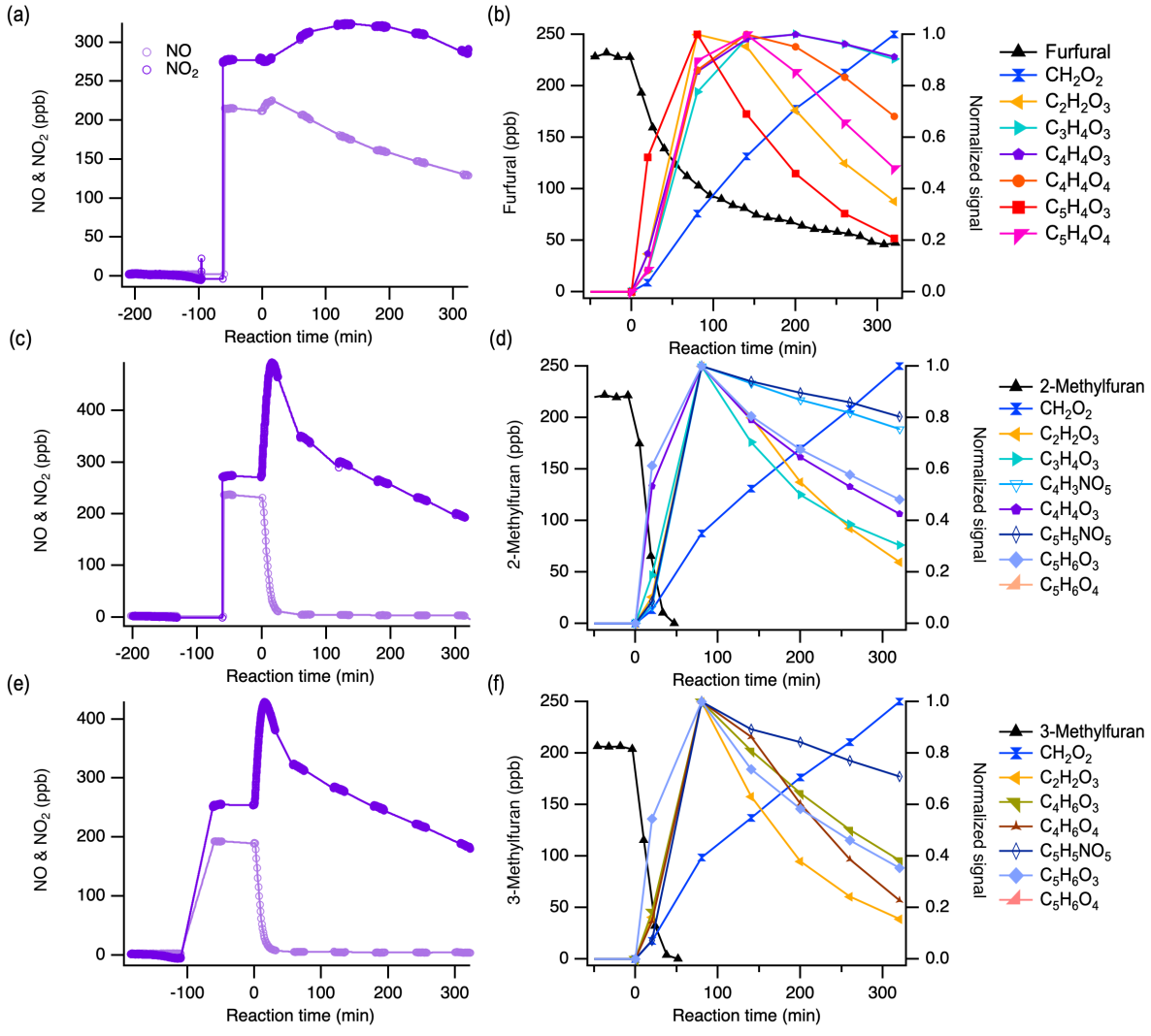

765

766 Figure 1. Temporal profiles of NO_x (a, c, e) and precursor VOCs (b, d, f) with gaseous oxidation
767 products during the photooxidation of furfural, 2-methylfuran, and 3-methylfuran, respectively. To
768 extend the experimental time, NO and NO_2 monitors sampled 15 mins continuously once every hour
769 and data points are interpolated between each measurement period.

https://doi.org/10.5194/egusphere-2026-4881
Preprint. Discussion started: 19 August 2026

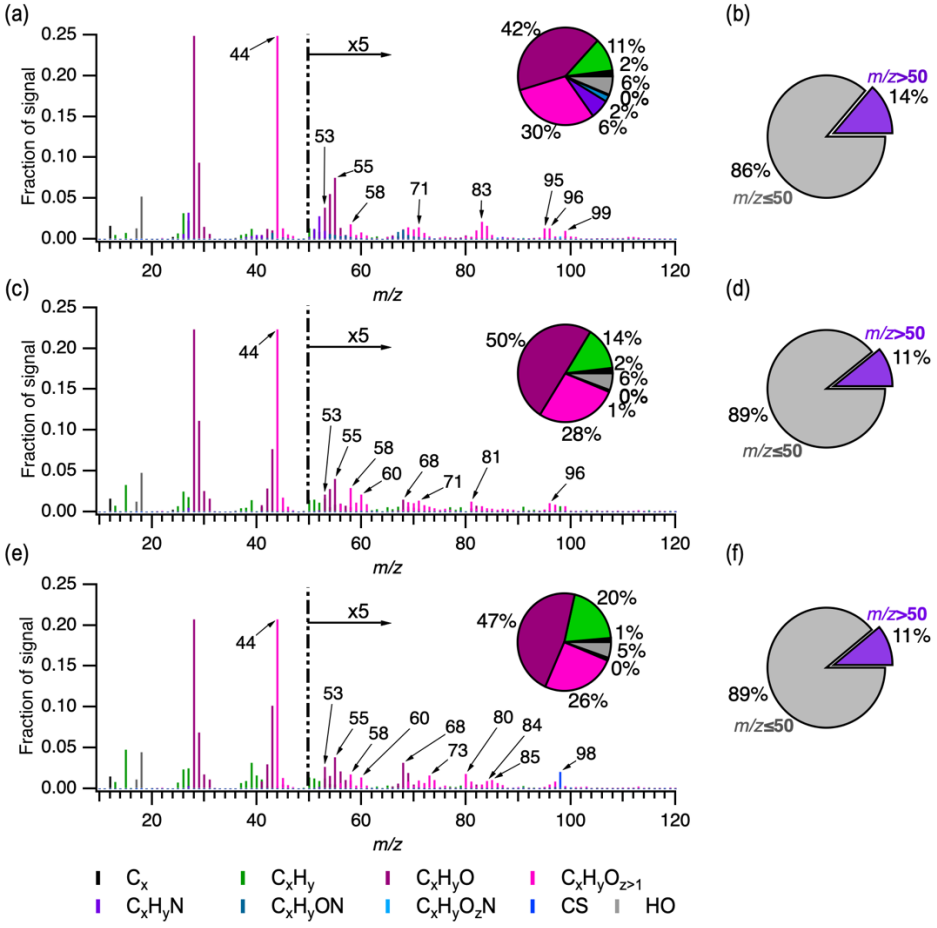

Figure 2. HR-ToF-AMS mass spectra and organic elemental composition of (a) furfural SOA, (c) 2-methylfuran SOA, and (e) 3-methylfuran SOA. Mass fractions of signals below (grey) and above (purple) *m/z* 50 (right panel) are shown for (b) furfural SOA, (d) 2-methylfuran SOA, and (f) 3-methylfuran SOA.

https://doi.org/10.5194/egusphere-2026-4881
Preprint. Discussion started: 19 August 2026

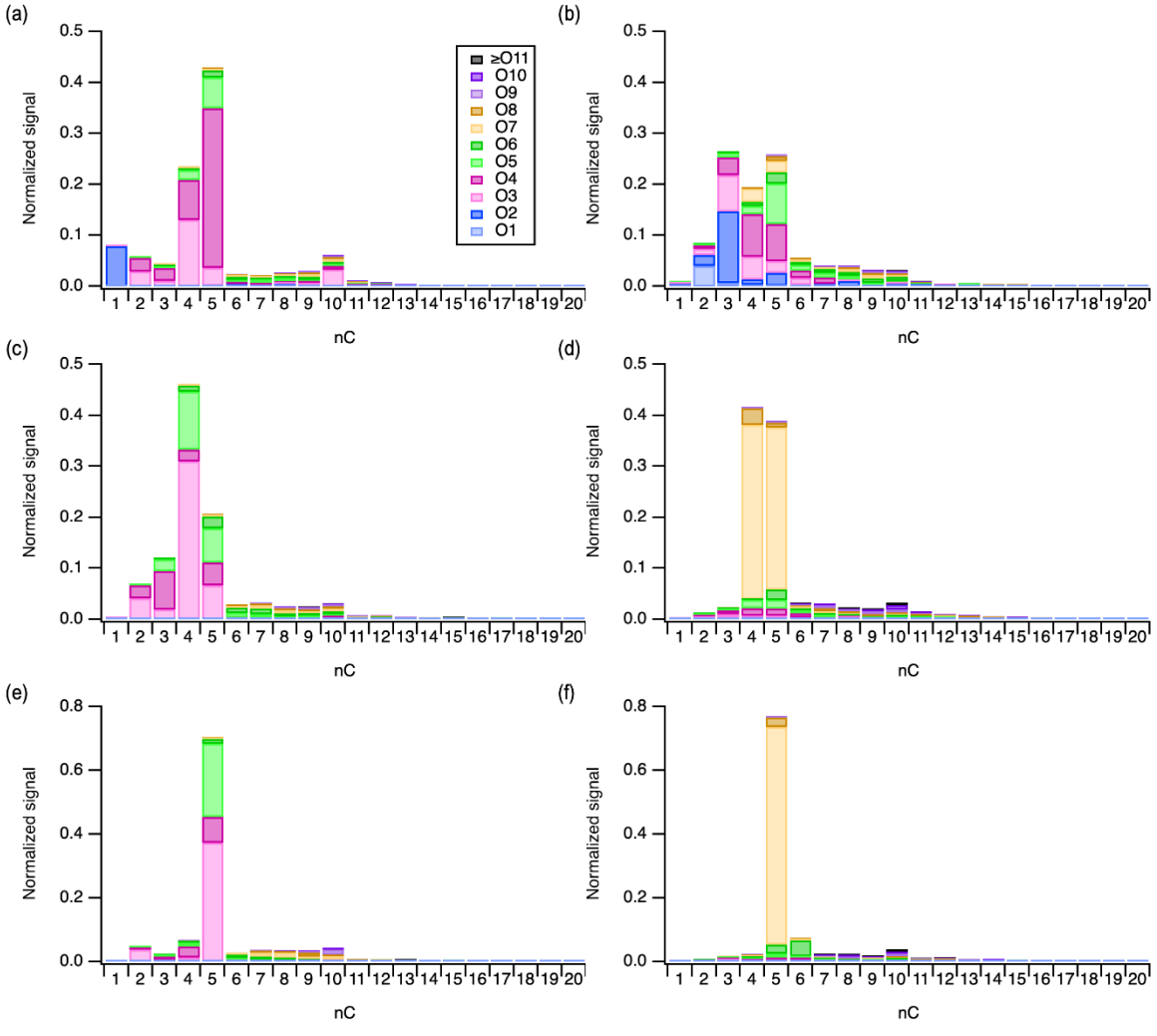

Figure 3. CHO (a, c, e) and CHON (b, d, f) compound classes in furfural SOA, 2-methylfuran SOA, and 3-methylfuran SOA, respectively, grouped by carbon and oxygen numbers, measured by FIGAERO-CIMS.

https://doi.org/10.5194/egusphere-2026-4881
Preprint. Discussion started: 19 August 2026

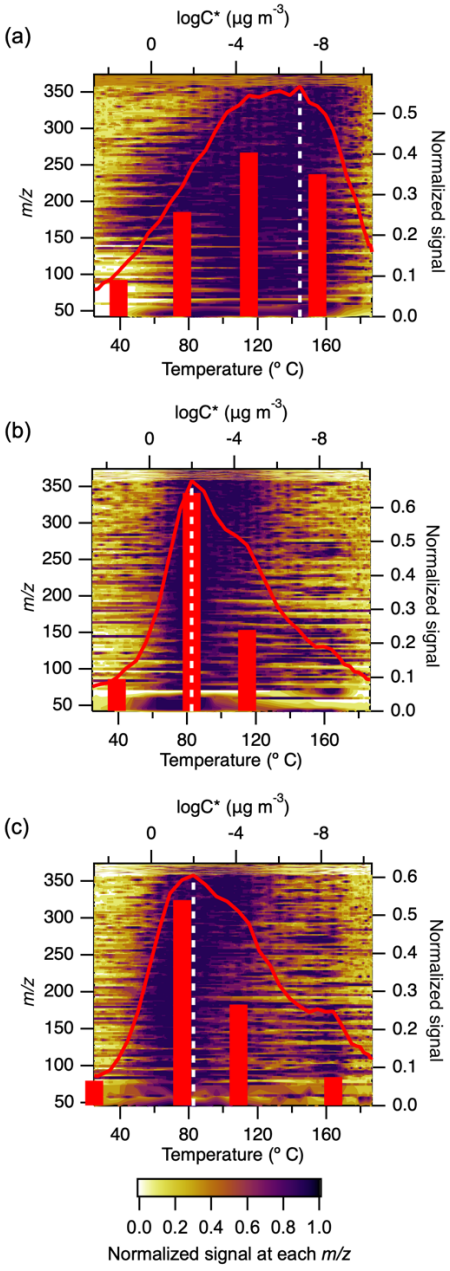

Figure 4. 2-D thermograms of (a) furfural SOA, (b) 2-methylfuran SOA, and (c) 3-methylfuran SOA. Solid red lines in 2-D thermograms are signal-weighted average thermograms, and red bars are estimated C* bins.

https://doi.org/10.5194/egusphere-2026-4881
Preprint. Discussion started: 19 August 2026

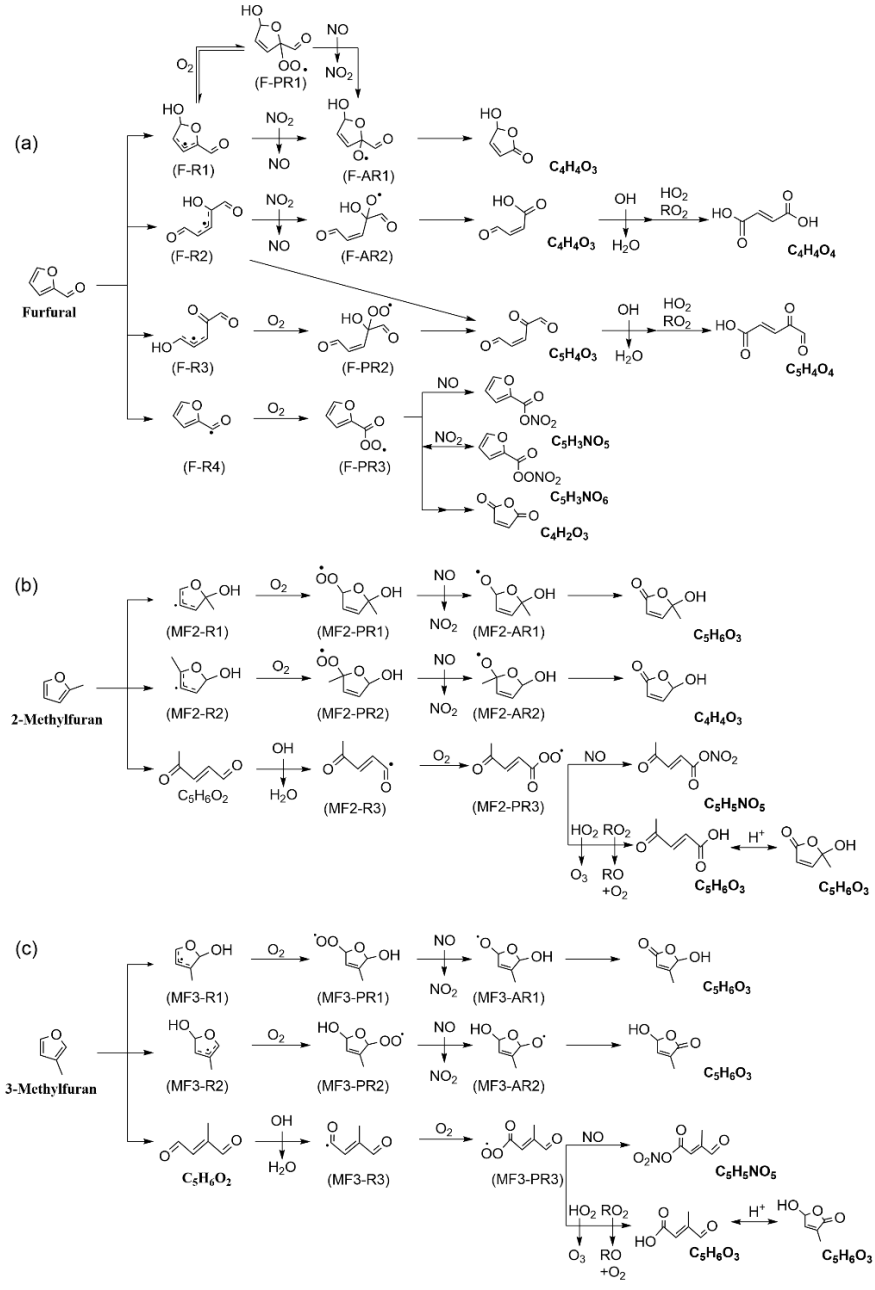

Figure 5. Simplified proposed oxidation mechanisms during (a) furfural+OH, (b) 2-methylfuran+OH, and (c) 3-methylfuran+OH experiments. More detailed oxidation mechanisms and additional second-generation product formation pathways are proposed in Figure S4.

https://doi.org/10.5194/egusphere-2026-4881
Preprint. Discussion started: 19 August 2026

787

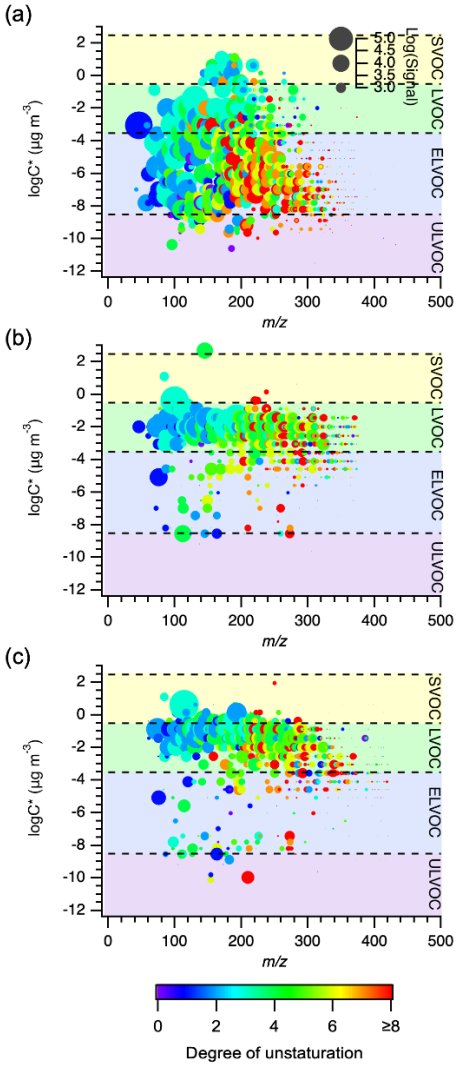

788

789 Figure 6. Saturation mass concentration (C*) vs. *m/z*, color coded by degree of unsaturation of
790 compounds detected in (a) furfural SOA, (b) 2-methylfuran SOA, and (c) 3-methylfuran SOA,
791 measured by FIGAERO-CIMS.

https://doi.org/10.5194/egusphere-2026-4881
Preprint. Discussion started: 19 August 2026

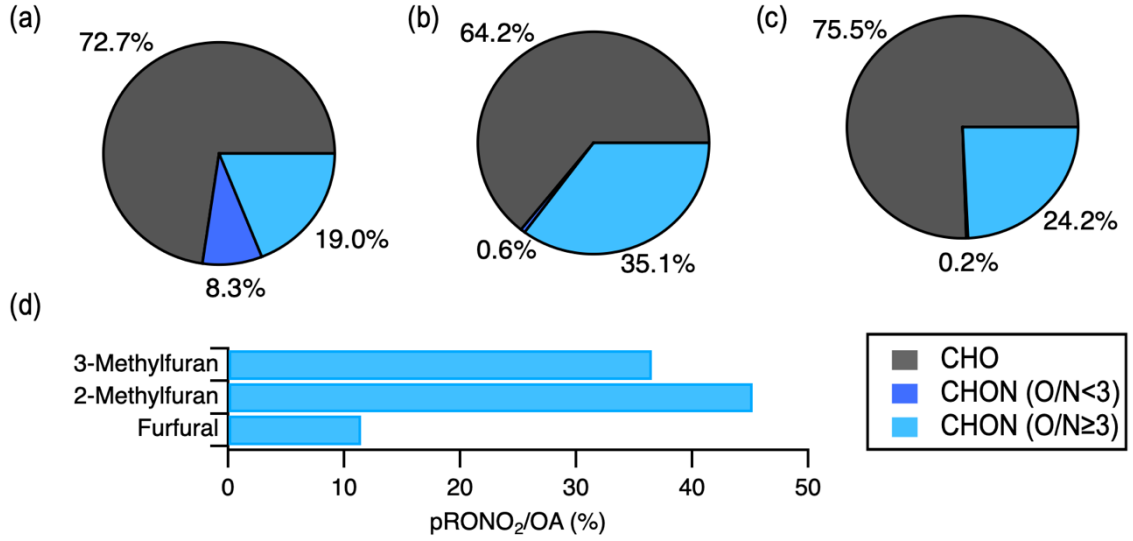

Figure 7. Different compound classes measured by FIGAERO-CIMS, weighted by signal intensity: (a) furfural SOA, (b) 2-methylfuran SOA, and (c) 3-methylfyran SOA. (d) Percentage of particulate organic nitrate ($pRONO_2$) in organic aerosol (OA) estimated from HR-ToF-AMS measurements with molecular weight information from FIGAERO-CIMS.

Table 1. Experimental conditions and SOA yields for all experiments.

Exp.	Precursor	Initial NO_x (ppb)	RH (%)	Injected VOC (ppb)*	ΔVOC (ppb)*	ΔM_o (μg m^{-3})**	SOA Yield (%)
1	Furfural	491.4	<5	228.9±1.8	172.4±1.8	66.3±1.0	9.8±0.05
2	2-methylfuran	506.1	<5	220.2±0.3	220.2±0.3	10.3±0.5	1.4±0.06
3	3-methylfuran	445.3	<5	205.5±0.3	205.5±0.3	7.2±0.5	1.1±0.07

* Uncertainties of VOC and consumed VOC (ΔVOC) are calculated based on the GC-FID calibration error and 1σ of VOC concentrations before onset of the photooxidation.
** Uncertainties for ΔM_o are calculated from 1σ of aerosol volume concentration measured by the SMPS at peak SOA mass concentration. Uncertainties in the SOA density are also propagated.